MINERALOGICAL MAGAZINE, VOL. 45, 1982, PP. 11–24

Exsolution structures in calcic pyroxenes from the Bjerkreim–Sokndal lopolith, SW Norway

F. J. M. RIETMEIJER

Department of Petrology, Instituut voor Aardwetenschappen, Budapestlaan 4, 3508 TA Utrecht, The Netherlands

AND

P. E. CHAMPNESS

Department of Geology, University of Manchester, Manchester M13 9PL

ABSTRACT. Iron-rich (Fs:En ~ 0.8) calcic pyroxenes that have been subjected to granulite-facies metamorphism contain up to seven generations of exsolution lamellae. They can be grouped into four stages. In stage 1 pigeonite exsolved parallel to '001' and '100' (where '*hkl*' signifies ~ (*hkl*)) and mostly inverted later to orthopyroxene. During stage 2 orthopyroxene exsolved parallel to (100), while during stage 3 orthopyroxene was quickly followed by metastable '001' pigeonite. The stage 3 precipitates clearly grew and thickened together for some time. During stage 4 a '100' pigeonite was exsolved. The stage 3 and 4 precipitates show evidence of reheating, dissolution and later, renewed growth. Sometimes orthopyroxenes of stage 3 have crossed a '001' pigeonite lamella and caused it to invert by a shear mechanism.

Chemical analysis shows no rotation of the tie lines between Ca-rich and Ca-poor phases, in contrast to previous studies of Skaergaard and Bushveld pyroxenes. The geothermometers of Wood and Banno (1973) and Wells (1977) indicate solidus temperatures of about 850 °C and 900 °C respectively, but the geothermometers were found to be unsuitable for subsolidus conditions. We estimate the pressure to have been about 9 kbar during solidification. Estimates of nucleation temperatures obtained from the orientations of the exsolved lamellae (Robinson *et al.*, 1977) were 850–700 °C for stage 1, and 600–400 °C for stage 3. We believe this geothermometer to be unreliable for the low temperatures involved in stage 4.

THE mechanism of precipitation (exsolution) and the nature of the subsolidus phases in lunar and terrestrial pyroxenes have been the subject of many studies in the past two decades. Extensive petrographic, single-crystal X-ray diffraction and, more recently, transmission electron microscopic (TEM) studies have shown that subsolidus phase relations in pyroxenes from slowly cooled igneous and metamorphic rocks may be complex (e.g. Ross *et al.*, 1972; Jaffe *et al.*, 1975; Robinson *et al.*, 1977; Rietmeijer and Champness, 1980*a*; and Nakajima and Hafner, 1980).

Robinson *et al.* (1971, 1977) have shown that the habit planes of exsolved Ca-rich and Ca-poor clinopyroxenes are not always parallel to (001) and (100) as had previously been assumed, but are (*h*01) planes that may deviate several degrees from the exact (001) and (100) orientations. The relative equilibrium cell dimensions of the phases are such that, for coherent exsolution of one phase from another, one principal strain is of opposite sign to the other two (the strain quadric is a hyperboloid). There are thus two directions perpendicular to the intermediate principal axis of strain (the *y*-axis) for which the strain is zero. Because the strain parallel to *y*, the elastic anisotropy and the chemical-energy component of the interfacial energy are small, the orientations of the exsolution lamellae are essentially those of the 'planes of best fit' at nucleation.

Robinson *et al.* (1971, 1977) showed that slowly cooled clinopyroxenes may contain several generations of lamellae, their differing orientations reflecting the change in the plane of minimum misfit at their nucleation temperatures. The change in relative unit-cell parameters of augite and pigeonite with temperature is largely the result of the $C \rightarrow P$ polymorphic transformation in pigeonite. This causes the *a* and *c* axes to decrease very rapidly near the temperature of transformation (Smyth, 1974). Robinson *et al.* (1977) used published cell dimensions and the augite–pigeonite solvi of Smith (1972) and Ross *et al.* (1973) to estimate the change in quilibrium lattice parameters with temperature for an augite from the Bushveld intrusion and the pigeonite exolved within it. From these data Robinson *et al.* calculated the expected variation of the habit planes of the '001'[1] and '100' lamellae with

[1] The symbol '*hkl*' indicates that the interface is approximately parallel to (*hkl*).

nucleation temperature and hence determined the exsolution temperatures of the observed lamellae.

The purpose of the investigation described in this paper was to reveal the exsolution structures produced in Ca-rich pyroxenes at extremely slow cooling rates with a view to understanding more fully the thermal history of the host rocks. The two samples described here are from the Bjerkreim–Sokndal lopolith, a layered intrusion associated with anorthosite masses (Michot and Michot, 1969). The igneous complex is part of the *HT–LP* granulite-facies metamorphic Precambrian terrane of Rogaland, SW Norway (Hermans *et al.*, 1975). Rietmeijer (1979) suggests that the intrusion may be subdivided into two major episodes, viz. the 'Leuconoritic' and (Quartz-)Monzonitic Phases (QMP). The former consists of melanocratic to leucocratic rocks in which orthopyroxene is a primary mineral, either as discrete, subhedral crystals or as discontinuous rims on Ca-rich clinopyroxenes. The QMP includes only leucocratic rocks in which the characteristic assemblages of Fe–Mg silicates are either Ca-rich clinopyroxene + Ca-poor clinopyroxene (± Fe-rich olivine) or Ca-rich clinopyroxene + fayalite + quartz. Pyroxene solidification for the QMP is bracketed at 1050–850 °C for P_{total} = 5–7 kbar at low P_{H_2O} (*c.* 0.5 kbar) and it is suggested that the orthopyroxene-bearing leucocratic rocks crystallized under similar conditions, albeit at a slightly higher total pressure (Rietmeijer, 1979). The cooling rate between 900–550 °C was estimated to have been about 7 °C/m.y. and between 550–400 °C about 2 °C/m.y. (Rietmeijer and Heijnen, in prep.).

In the metamorphic terrane surrounding the intrusion Kars *et al.* (1980) recognized four succes-

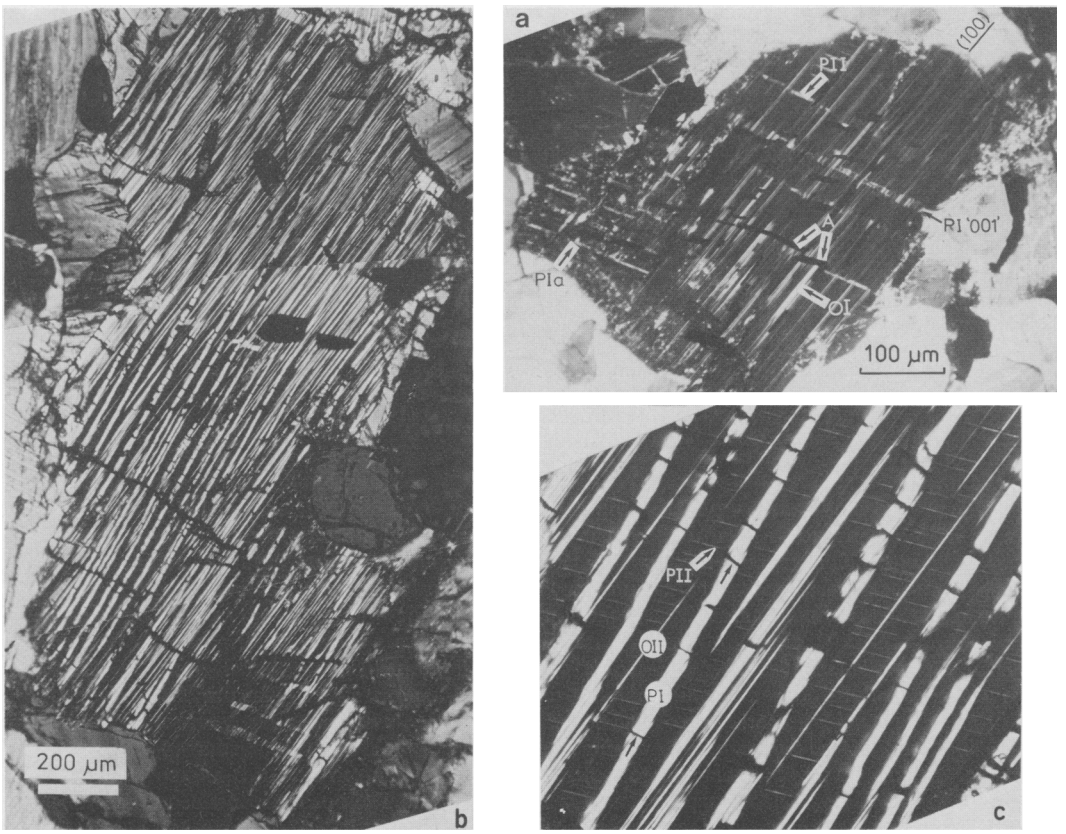

FIG. 1. Optical micrographs (crossed polars) of (010) sections of Ca-rich pyroxenes from Rogaland. (*a*) R340, showing OI, PI '001', PIa, OII (parallel to (100) especially in top RH corner), and PII lamellae. Note the Fe–Ti oxides parallel to '001' and '100'. Those at A appear to have nucleated OI lamellae. (*b*) A grain of R394 showing PI '001' (bottom right), PI '100' (wider NE–SW lamellae), and OI (at about 4° to PI). (*c*) Higher magnification micrograph of the centre portion of grain in (*b*) showing PI, OII, and PII lamellae. The opaque phase in the PII lamellae is probably magnetite.

sive stages of regional metamorphism, viz. M1 around 1200 Ma (including a period of syenitic magmatism); M2 at about 1050 Ma induced by the intrusion of the lower part of the Bjerkreim–Sokndal lopolith; M3 a cooling period between 950–800 Ma down to about 400 °C (Verschure *et al.*, 1980) and M4 at about 400 Ma, probably related to the Caledonian orogenesis. The M4 stage is of low metamorphic grade (prehnite-pumpellyite-facies and locally green biotite).

Both samples studied, R340 and R394 (NGU grid coordinates 3494-64768 and 3453-64775), are olivine–hypersthene monzonites from the QMP. Textural evidence in R394 suggests that pyroxene solidification may have been close to the three-phase field (opx–pig–aug), defining an invariant assemblage in the pseudo-binary pyroxene T-X(Wo) diagram (e.g. Ross and Huebner, 1975).

Pyroxene exsolution structures

General description. Optical and electron petrography of the augites reveals up to seven generations of precipitates, although any one crystal rarely contains all seven. Consideration of their relative distribution and the known stability relationships among pyroxenes, as discussed below, has allowed us to recognize four stages of exsolution with decreasing temperatures (Table I).

Stage 1 consists of three generations of lamellae that mostly nucleated on grain boundaries or on exsolved Fe–Ti oxides. Two of the generations are parallel to '001' (PI '001' and PIa) and the third is parallel to '100' (PI '100', fig. 1). Two, or even three, of the stage 1 precipitates may occur in the same grain of augite, but usually one of them is dominant; PI '001' is the most common. When more than one precipitate from stage 1 is present, they usually occur in distinct domains within the augite, with the '100' lamellae tending to be near the centre of the grain (Rietmeijer, 1979). The presence of the domains suggests that the lamellae of stage 1 nucleated at similar temperatures. Occasionally PI '001' lamellae appear to change direction at a late stage in their growth and become parallel to '100' (Rietmeijer, 1979, p. 102). This suggests that PI '100' precipitated at a lower temperature than PI '001' or PIa.

All three lamellae were initially pigeonites. Apart from PI '100' and PI '001' lamellae that are thinner than about 6 μm, all have inverted to orthopyroxene. The directions of the y and z axes were retained during the inversion and augite lamellae were later exsolved parallel to $(100)_{opx}$. All the precipitates of stage 1 have lost coherency with the augite matrix.

Stage 2 of the precipitation sequence consists of a single generation of orthopyroxene lamellae, OI, parallel to (100). They nucleated at grain boundaries or at the interfaces between the (now) inverted pigeonite lamellae of stage 1 and the matrix (cf. the nucleation of augite lamellae at '001' and '100' augite boundaries in inverted pigeonites from Rogaland; Rietmeijer and Champness, 1980*b*).

In the regions where the spacing between OI and PI '100' lamellae is greater than about 1.2 μm, the augite matrix contains precipitates of stages 3 and 4 (figs. 1 and 2). Stage 3 consists of two phases.

TABLE I. *Orientation and size of the exsolution lamellae in augite*

Stage	Type of lamella	Thickness range (microns)	Angle between interface and (100) augite	
			Sample R340	Sample R394
1	PI '001'	3–40	105.5°	105.0°
	PIa '001'	~ 5	110.5°	—
	PI '100'	⩽ 10	—	−4°
2	OI (100)	0.15–1.0	0°	0°
3	OII (100)	< 0.005–0.6	0°	0°
	PII '001'	0.1–0.5	113.5°	112–116°
4	PIII '100'	< 0.005–0.1	0°	~2 → +9°

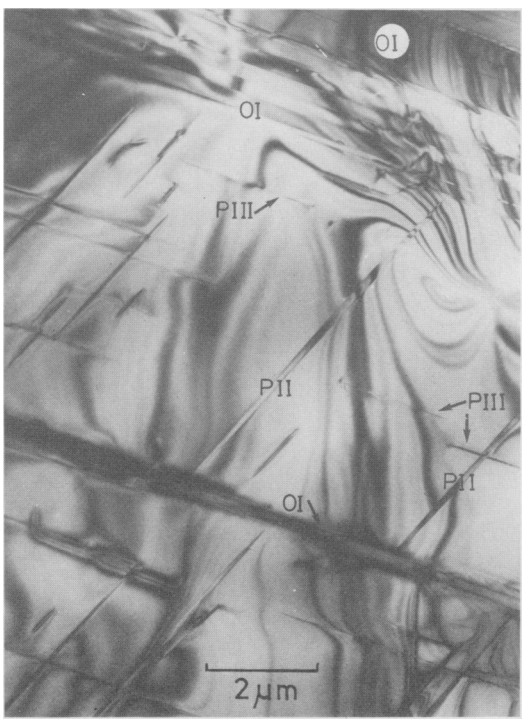

FIG. 2. Electron micrograph (1000 kV) of augite from R394. PII and PIII lamellae occur between widely spaced OI lamellae. *All electron micrographs are (010) sections.*

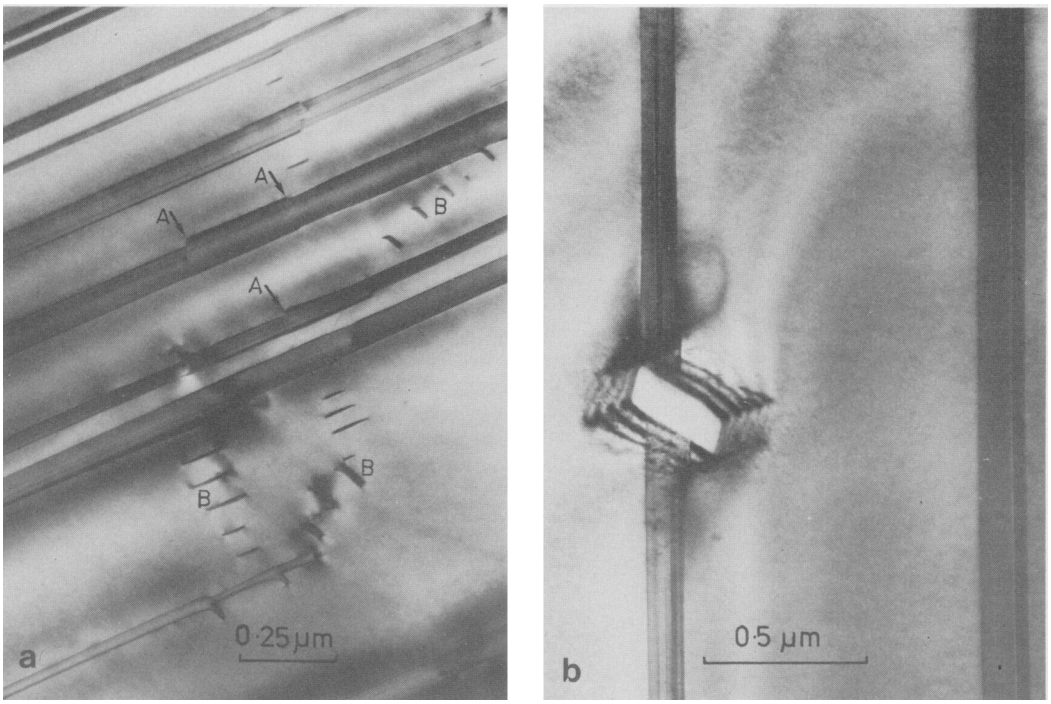

FIG. 3 (*a*). OII lamellae on which late-stage pigeonite has nucleated. Growth of the pigeonite was held up, in many cases, by the dislocations of a sub-grain boundary (e.g. at A). '001' and '100' pigeonites (PII and PIII) have also nucleated on dislocations in the subboundary (e.g. at B). (*b*) An OII lamella has nucleated on a particle of apatite (identified by AEM). Sample R340.

Orthopyroxene, OII, is semicoherent with the augite and parallel to (100). Both orthopyroxenes, OI and OII, thickened by the propagation of ledges that are normally 18 Å high. Pigeonite,[1] PII, the other phase in stage 3, is coherent and parallel to '001'. PII lamellae are lens-shaped, being widest mid-way between the OI lamellae (fig. 2). This indicates that a solute profile was produced during thickening of OI and that PII nucleated where the supersaturation was highest.

Thin, coherent pigeonite lamellae, PIII, are parallel to '100' and constitute stage 4. We believe that all the pigeonites of stages 2, 3, and 4 nucleated in the stability field of orthopyroxene, below the pigeonite to orthopyroxene inversion temperature. Thus the pigeonites nucleated metastably at temperatures that were too low for the nucleation of the stable phase (cf. Jaffe *et al.*, 1975). (Orthopyroxene has a structure that differs significantly from that of the matrix. The activation energy needed for its nucleation is therefore very much higher than for pigeonite whose structure is very similar to that of augite.) Metastable pigeonite has also been found to precipitate by spinodal decomposition at high temperatures in diopsides from kimberlites (McCallister and Nord, 1981).

Isaacs and Peacor (1981) have suggested that pigeonite was a precursor to orthopyroxene exsolution in augite at relatively low temperatures in Adirondack granulites. We reject that possibility for the OI and OII orthopyroxene lamellae in the Rogaland augites for two reasons. First, in all cases the lamellae are exactly parallel to (100), as can be seen by viewing the (100) lattice fringes. Our calculations (see fig. 11) show that pigeonite would only have this orientation for a nucleation temperature of about 600 °C. However, as later discussion will show, the evidence suggests that OI exsolved at a considerably higher temperature. Our second reason for rejecting Isaacs and Peacor's suggestion for the Rogaland pyroxenes is that PII lamellae, which are often much wider than OII lamellae, have not inverted to orthopyroxene, although they have a similar Ca content to OII.

The orthopyroxene lamellae of stages 2 and 3 contain thin (100) lamellae (figs. 3*a*, 3*b*, 4*a*, 5).

[1] We use this term to imply a Ca-poor clinopyroxene that is isostructural with augite at high temperatures, but has space group $P2_1/c$ at low temperatures (cf. Huebner, 1980). The Wo content may be 0–15%.

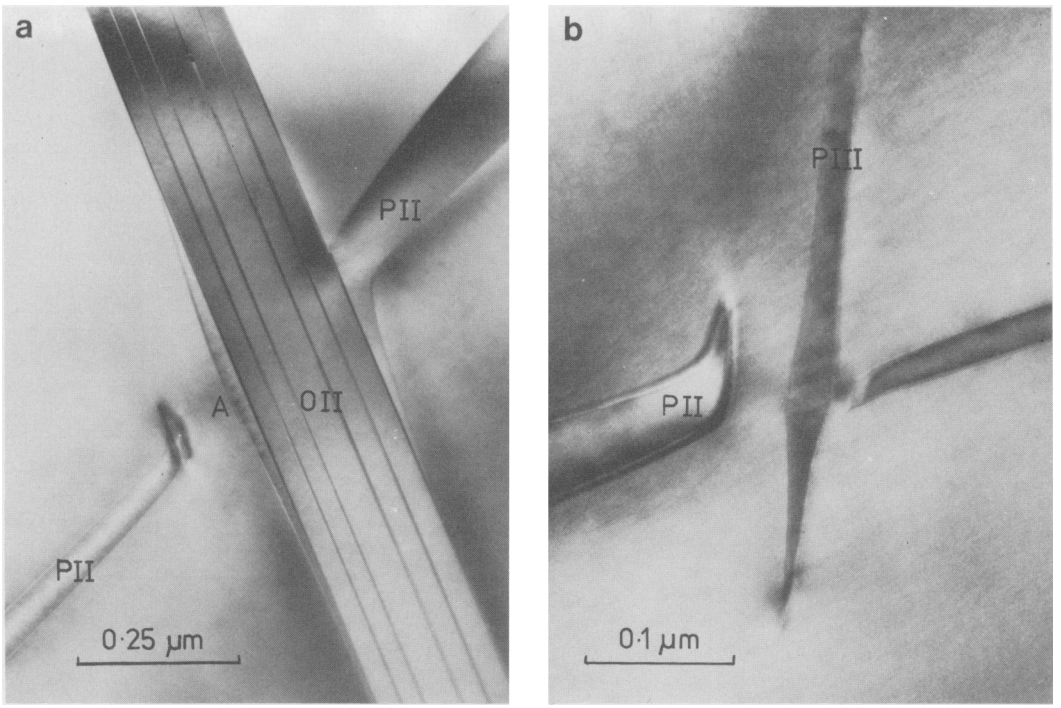

FIG. 4. Interaction between precipitates of stage 3. (*a*) Two PII lamellae are aligned across an OII lamella. Notice the change in habit plane of the PIIs, the 'bulge' of pigeonite at A, and the thin (100) lamellae within OII. (*b*) Two PII lamellae are aligned across a PIII lamella. Notice the 'bulge' in PIII. Sample R394.

Resolution of the (100) lattice planes reveals a spacing of 9 Å within them, consistent with their being pigeonite (fig. 5). Diffraction patterns from OII lamellae that have a high density of (100) lamellae confirm this. The thin lamellae can be either an odd or an even number of 9 Å units wide, but 27 Å is the most common width. We have used the convention of Buseck and Iijima (1975) for measuring the width and we have made measurements only where the thickness and orientation of the sample are constant. In fig. 5 there are two lamellae 27 Å wide. Inset is a schematic representation of the structure which shows that the lamellae contain an extra unit cell of pigeonite inserted within the orthopyroxene. Lamellae that are odd multiples of 9 Å wide clearly cannot have formed directly from the orthopyroxene because the latter is out of step across such a lamella. The pigeonite must, therefore, have formed from a structure within a 9 Å (100) repeat, i.e. from augite as the orthopyroxene was growing within it rather than by shear of, or precipitation from, the orthopyroxene. The presence of two orientations, as revealed by differences in diffraction contrast between lamellae in regions where the diffracting conditions are constant (e.g. fig. 5), indicates that the two possible twin orientations of the monoclinic unit cell are present (inset, fig. 5). This could not have occurred if the pigeonite had formed by shear of the orthopyroxene (see Buseck *et al.* (1980) for a discussion of the criteria for determining how clinopyroxene formed).

The lamellae that are 27 Å wide, such as in fig. 5, could be growth faults that formed by the propagation of 9 Å ledges during thickening of the orthopyroxene. However, this explanation is unlikely for the wider ones. Presumably they are pigeonite that formed metastably at temperatures where it was becoming difficult for the transformation of augite to orthopyroxene to take place. (Nord and McGee (1979) also reported intergrowths of pigeonite and orthopyroxene parallel to (100) in a lunar augite. However, in that case the pigeonite probably formed as a result of later deformation of the rock.)

The precipitates of stages 3 and 4 nucleated on sites within the augite grain. Fig. 3*a* shows a number of PII and PIII pigeonites that nucleated either on the dislocations of a sub-boundary or on the interface of OII lamellae. In fig. 3*b* an OII

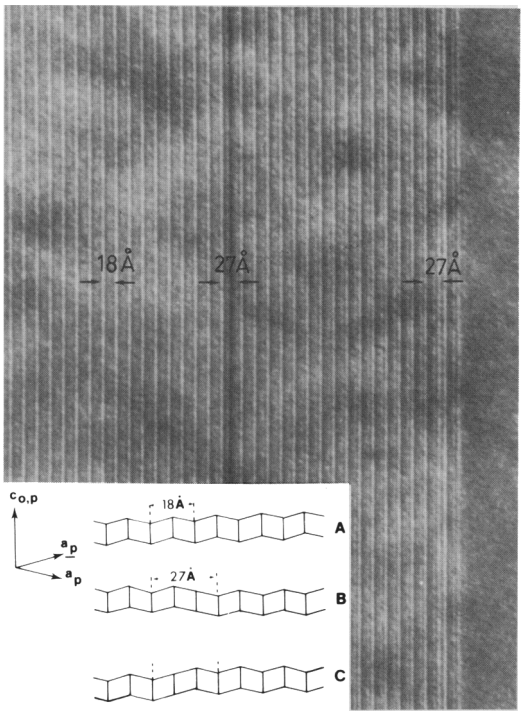

FIG. 5. High-resolution micrograph of an OII lamella containing two (100) lamellae 27 Å wide. Inset is a diagram of the structure of the 'faults' which shows that they contain an extra half unit cell of orthopyroxene (equivalent to one unit cell of pigeonite). The contrast difference between the two shows that the pigeonite cells are twin-related. Sample R394.

lamella has nucleated on an inclusion of apatite; nearby a '100' pigeonite (PIII) nucleated on another apatite inclusion.

The PII lamellae change their habit plane to '100' at their extremities (figs. 2, 4) and occasionally in other places. The direction of growth of the '100' segment is always such that there is an obtuse angle between it and the '001' segment. Champness and Lorimer (1982, fig. 7*b*) have suggested that this occurs so that the '100' segment does not grow into the zone previously depleted of solute by the '001' segment. The change in habit plane of PII often takes place at the interface of an OI or OII lamella (fig. 4*a*). The fact that the last stage of growth of PII is along '100' leads us to the conclusion that '100' is the preferred habit plane at the lowest temperatures of precipitation and is the reason that we have assigned PIII (and the '100' segment of PII) to the separate, later stage 4. PIII precipitates, when they encounter a PII lamella, continue to grow along the interface of the latter (Rietmeijer and Champness, 1980*a*, fig. 4), but never otherwise show a change in habit plane to '001'. However, a number of very thin PIII lamellae in R394 are curved and have changed their inclination to (100) during growth by up to 3°.

The PII lamellae, like the orthopyroxenes, contain thin (100) lamellae (fig. 6). These are stacking faults with a fault vector of 1/6 *c* (Champness and Copley, 1976) and form in coherent, '001' pigeonite lamellae to relieve the strain caused by the differential contraction of the augite matrix compared with that of the pigeonite (particularly the decrease in β) (Robinson *et al.*, 1977). The sense of the shear involved is the reverse of that which occurs in the orthopyroxene lamellae.

The (100) faults in coherent pigeonite lamellae may form nucleation sites for the inversion to orthopyroxene (Champness and Copley, 1976). The faults also form in incoherent pigeonite lamellae or matrices as a precursor to the inversion reaction (see Nobugai *et al.*, 1978, fig. 4). The density of faults in coherent pigeonites depends upon the thickness of the lamella, even within the same generation of lamellae, so cannot be used as a relative geothermometer as suggested by Robinson *et al.* (1977).

Interaction between precipitates. It is quite common for PII lamellae to be aligned approximately along '001' across an OII or a PIII lamella

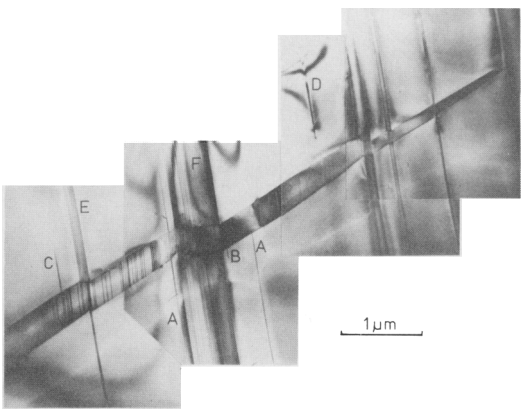

FIG. 6. The interaction of a PII lamella with several OII lamellae. The latter may be only a few unit cells wide, cf. the two lamellae marked A. One of these enters PII, but does not re-emerge. Note the (100) stacking faults in the pigeonite and the variation in their density with the width of PII. A small lamella of orthopyroxene appears to have been nucleated at one of these faults and grown into the augite at B. On the far right is a PIII lamella. A small PIII lamella meets PII at C, whereas that at D does not. Electron diffraction of lamella E shows that it contains pigeonite and orthopyroxene. Note the semicoherent interface, approximately parallel to $(001)_{opx}$, between the thick OII lamella F and PII. Sample R340.

(figs. 4 and 6). In fig. 4*a* one of the PII lamellae has grown along the orthopyroxene interface, but the other changes its habit plane before it meets the orthopyroxene. However, there is a 'bulge' of pigeonite along the orthopyroxene interface on this side. Such a 'bulge' invariably accompanies the termination of a PII lamella just before it reaches an OII interface. Fig. 4*b* shows a similar, fairly common, interaction between two PII lamellae and a PIII lamella. Once again the '001' precipitates are aligned. Neither PII meets the PIII pigeonite, but the latter is thicker at the point closest to the '001' lamellae. These observations lead us to conclude that the microstructures may be the result of reheating and cooling, possibly during the M4 stage of regional metamorphism. The two PII lamellae in figs. 4*a* and *b* may once have been one lamella parallel to '001'. The OII lamella in fig. 4*a* may have passed through PII and initiated inversion to orthopyroxene within it (see below). The three lamellae in fig. 4*b* may once have been intergrown like the PII and PIII lamellae in fig. 4 of Rietmeijer and Champness (1980*a*). Reheating to a temperature within the orthopyroxene stability field could have resulted in dissolution of some of the metastable pigeonite and, possibly, further growth of orthopyroxene. The dissolution would have occurred preferentially where the lamellae were thinnest, causing separation of the PII lamellae in fig. 4 into two lamellae, but leaving behind a small 'bulge' where the pigeonite had 'wet' the orthopyroxene. Later cooling to a temperature at which the orthopyroxene could no longer thicken would result in renewed growth of the metastable pigeonites, and eventually they would grow along '100', either in the matrix or along the orthopyroxene interface. Thus the stage 4 precipitation may have taken place entirely during the M4 metamorphic event.

OII and PII lamellae show a number of features that suggest that they grew and thickened simultaneously for part of their lives (which is the reason we have placed them in the same stage). For instance, in fig. 7 an OII lamella encountered a PII lamella and stopped growing at A. Towards the bottom of the figure, at B, the same PII lamella encountered another OII lamella and continued to grow along the (100) interface (cf. fig. 4*a*) after the orthopyroxene had ceased thickening.

In most cases where an OII lamella has met a PII lamella, it has 'grown through' the pigeonite, by causing the latter to invert, and continued to grow on the other side (figs. 6, 8, and fig. 3 of Rietmeijer and Champness 1980*a*). The orthopyroxene lamellae may only be a few unit cells wide, as at A in fig. 6, and may be overgrown by late pigeonite (cf. fig. 3*a*). As the orthopyroxene passes through the pigeonite its orientation changes by about 3° due to the change in orientation of the (100) plane in augite compared with pigeonite.

The orthopyroxene, where it has passed through a pigeonite lamella, appears to have caused the latter (and the matrix) to be displaced along (100), the displacement being very roughly equal to the width of orthopyroxene that passes through the pigeonite. The orthopyroxene and primitive clinopyroxene structures are related by a shear on (100) along the *z* axis. McLaren and Etheridge (1976) studied the transformation of ortho- to clinopyroxene in a naturally deformed sample (the reverse of the transformation being considered here). They showed that the two structures are related by a fault of 0.17 *c* every 18 Å along x*, but they could not distinguish between Burgers vectors of ± 1.17 [001] and ± 0.83 [001] for the leading partial dislocation. In the present case the displacement[1]

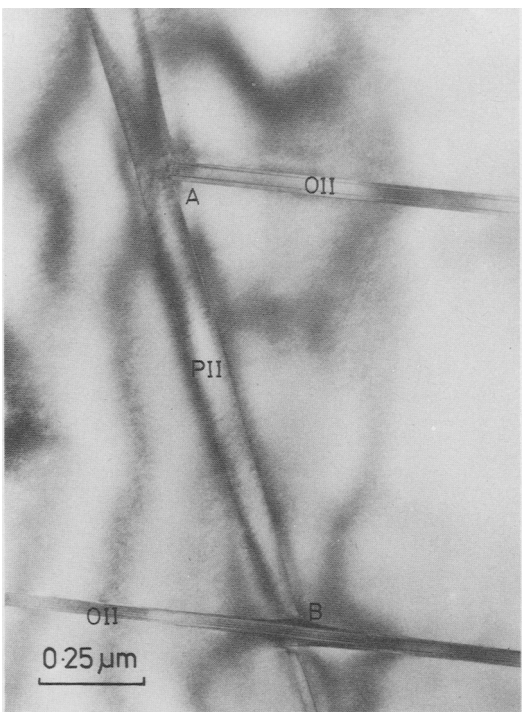

FIG. 7. Interaction between a PII lamella and two OII lamellae. Sample R340.

[1] The faults that occur in the pigeonites to relieve the strain caused by coherence do not produce a macroscopic shear of the lamella. This is to be expected from the McLaren–Etheridge model because the effect of two adjacent faults is a slight rotation of the lattice without a change in the trace of the '001' interface (see Nobugai and Morimoto, 1979, fig. 6).

of the pigeonite lamellae is in the direction predicted by the McLaren–Etheridge mechanism (compare figs. 6 and 8 with their fig. 2*b*) and the orthopyroxene advances through the augite and into the pigeonite by the migration of ledges 18 Å high (fig. 8), but the magnitude of the displacement of the pigeonite cannot be accounted for solely by the passage of a partial dislocation of Burgers vector ± 1.17 [001] or ± 0.83 [001]. Burgers vectors 2.17 [001] or 2.83 [001] would give displacements of the right order, but are most unlikely due to their high energy. In the region of the intersection, the pigeonite lamellae have thickened more extensively along the interface that makes an obtuse angle with the crossing orthopyroxene lamella than along the opposite interface (the pigeonite usually forms a '100' overgrowth in the former case, rarely in the latter). This will have occurred for the same reason that the '001' and '100' sectors of PII lamellae always form an obtuse angle, i.e. because of the effect on the availability of solute of the presence of the orthopyroxene. The effect is most convincingly demonstrated by area A of fig. 7, where the orthopyroxene does not cross the pigeonite and there is thus no displacement of the pigeonite interface that is not in contact with the orthopyroxene, although there is a marked effect on the other side. This phenomenon will have the effect of enhancing the apparent displacement of the pigeonite relative to the orthopyroxene. We do not believe, however, that it could be the only cause of the displacement; a very thick orthopyroxene lamella, such as in fig. 6, displaces the pigeonite too much.

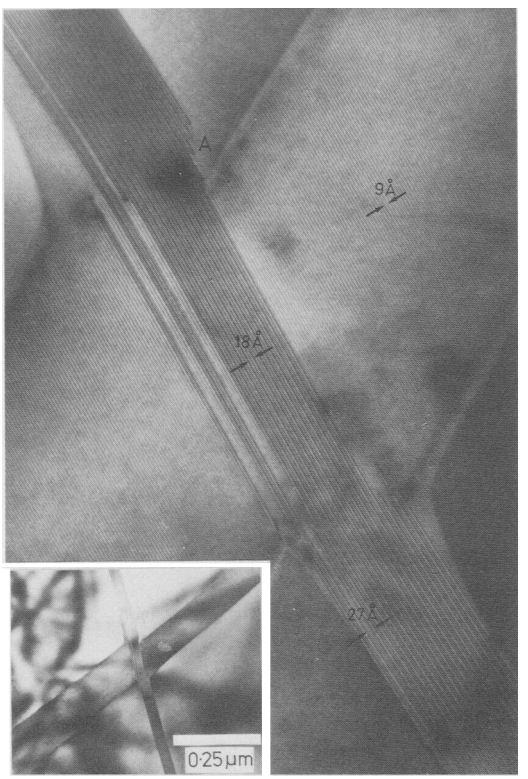

FIG. 8. An OII lamella has crossed a PII lamella and caused it to invert. The (100) lattice fringes are resolved in the orthopyroxene (~ 18.3 Å) and the pigeonite (~ 9.2 Å). Note the ledges on the OII interface at A and the faults in the stacking of the (100) planes of orthopyroxene (cf. fig. 5). Inset is a micrograph, taken at lower magnification, that shows the displacement of PII across OII. Sample R340.

Nord and McGee (1979) found that (100) deformation twins in a lunar augite pass through '001' exsolution lamellae of pigeonite. However, their fig. 6*a* shows that, although a slight displacement of the pigeonite lamella occurs, its magnitude is smaller than in the present case. This is the reverse of what would be expected if the apparent displacement in the Rogaland pigeonites is due solely to the shear involved in the reaction, assuming that the same partial dislocation is involved in the two cases. Twinning requires that a partial dislocation passes through the clinopyroxene structure every 9 Å along x^* (i.e. twice as often as is needed to produce orthopyroxene).

Chemical data

Analyses of solidus and subsolidus phases have been carried out using a conventional electron microprobe analyser (Rietmeijer, 1979) and an analytical electron microscope (EMMA-4). The absolute error in microprobe analysis for oxides (expressed in weight per cent) are: $SiO_2 \pm 0.5$; Al_2O_3 ± 0.15; $TiO_2 \pm 0.01$; $FeO \pm 0.4$; $MnO \pm 0.08$ (for Opx) and ± 0.02 (for Ca-Cpx); $MgO \pm 0.3$; CaO ± 0.2, and $Na_2O \pm 0.055$. The error in EMMA-4 analyses is: $SiO_2 \pm 1.0$; $Al_2O_3 \pm 0.4$; $FeO \pm 0.85$; $MnO \pm 0.1$; $MgO \pm 0.4$; $CaO \pm 0.8$ (TiO_2 and Na_2O were not detected).

The advantages of thin-foil analysis over conventional microprobe analysis is that, for probe sizes down to about 0.01 μm and foil thicknesses of about 0.1 μm at 100 kV, the analysed area of a silicate is approximately the area of the incident probe. In the present case the minimum probe size used was about 0.15 μm. Thus the probe size was too large to allow PIII lamellae to be analysed. To a first approximation, for the elements of interest here and the sample thicknesses examined, absorption and fluorescence could be neglected (for a recent review of AEM see Champness *et al.*, 1981).

The chemical analyses are given in Table II and are plotted on part of pyroxene quadrilateral in

TABLE II. Chemical analyses of pyroxenes and olivine in samples R 394 and R 340

analyses no.	394-1*	394-2**	394-3*	394-4	394-5*	394-6*	394-7*	394-8**	394-9*	394-10	394-11*	394-12**	394-13*	394-14**	394-15**
SiO_2	47.0	47.0	46.7	48.3	48.5	48.7	48.6	49.7	46.7	49.0	46.6	47.8	50.1	48.0	48.1
Al_2O_3	1.75	nd	1.3	1.3	1.2	1.4	1.4	0.7	1.2	0.8	1.2	0.8	0.7	0.3	0.7
TiO_2	0.1	nd	0.1	0.2	0.2	0.2	0.4	nd	0.2	nd	0.1	nd	nd	nd	nd
FeO	44.6	45.0	43.4	30.4	29.5	27.65	26.8	27.7	37.0	34.0	38.0	44.5	23.6	45.2	44.5
MnO	1.0	1.3	0.9	0.6	0.6	0.5	0.6	0.9	0.8	0.8	0.9	0.9	0.6	1.3	1.0
MgO	5.1	6.1	4.9	4.6	4.6	4.6	4.5	4.2	4.6	4.6	4.8	5.0	4.3	4.5	4.7
CaO	1.4	0.6	2.8	14.8	15.9	16.8	18.2	16.8	10.1	10.5	8.2	1.0	20.3	0.8	0.9
Na_2O	0.4	nd	0.2	0.5	0.5	0.5	0.6	nd	0.3	nd	0.2	nd	nd	nd	nd
total	101.35	100.0	100.3	100.7	101.0	100.35	101.1	100.0	100.9	99.7	100.0	100.0	99.6	100.1	99.9
Si	1.95	1.98	1.95	1.95	1.95	1.96	1.95	2.00	1.93	2.00	1.94	2.00	2.01	2.01	2.01
Al	0.05	0.00	0.05	0.05	0.05	0.04	0.05		0.06		0.06				
Al	0.04	0.00	0.01	0.01	0.01	0.03	0.02	0.03		0.04		0.04	0.03	0.015	0.03
Ti	0.00	0.00	0.00	0.01	0.01	0.01	0.01	0.00	0.01	0.00	0.00	0.00	0.00	0.00	0.00
Fe^{2+}	1.54	1.58	1.52	1.03	0.99	0.93	0.90	0.94	1.27	1.16	1.32	1.56	0.79	1.585	1.56
Mn	0.04	0.05	0.03	0.02	0.02	0.02	0.02	0.03	0.03	0.03	0.03	0.03	0.02	0.04	0.04
Mg	0.31	0.38	0.30	0.28	0.28	0.27	0.27	0.25	0.28	0.28	0.30	0.31	0.26	0.28	0.29
Ca	0.06	0.03	0.13	0.64	0.69	0.72	0.78	0.73	0.45	0.46	0.37	0.045	0.87	0.035	0.04
Na	0.03	0.00	0.02	0.04	0.04	0.04	0.05	0.00	0.02	0.00	0.02	0.00	0.00	0.00	0.00
total	4.02	4.02	4.01	4.03	4.04	4.02	4.05	3.98	4.05	3.97	4.04	3.985	3.98	3.965	3.97
En	16.2	19.2	15.4	14.4	13.8	14.1	13.8	13.0	14.0	14.7	15.1	16.2	13.5	14.7	15.4
Fs	80.6	79.4	77.9	52.8	50.8	48.4	46.2	49.0	63.5	61.1	66.3	81.5	41.1	83.4	82.5
Wo	3.2	1.4	6.7	32.8	35.4	37.5	40.0	38.0	22.5	24.2	18.6	2.3	45.4	1.9	2.1
Fe/(Fe+Mg)	0.83	0.81	0.84	0.79	0.79	0.77	0.77	0.79	0.82	0.81	0.81	0.83	0.75	0.85	0.84
N		1						1				1	1	1	4

analysis no.	394-16**	394-17**	394-18**	340-1*	340-2*	340-3	340-4*	340-5*	340-6*	340-7**	340-8**	340-9 **	340-10*	340-11**	340-12
SiO_2	50.9	51.5	47.2	47.3	47.9	49.35	49.1	49.2	47.5	47.4	50.0	50.1	49.8	48.0	30.7
Al_2O_3	0.5	1.0	0.5	0.6	0.5	1.2	1.2	1.6	0.9	0.65	1.2	1.1	1.4	0.9	0.2
TiO_2	nd	0.1	nd	0.2	0.2	0.2	0.2	nd	nd	nd	nd	nd	0.2	nd	0.1
FeO	24.0	22.7	45.1	41.7	43.5	24.95	23.8	34.6	42.9	44.0	22.5	21.5	23.0	43.8	65.2
MnO	0.2	0.4	1.1	0.85	0.9	0.4	0.5	na	na	1.15	0.5	0.6	0.4	1.2	1.2
MgO	4.7	4.3	5.2	7.4	6.8	5.85	5.6	6.2	6.8	6.0	5.9	5.3	5.9	5.4	3.6
CaO	19.7	20.0	0.85	1.0	0.9	17.15	17.8	6.5	0.7	1.15	19.9	21.5	19.4	0.8	0.1
Na_2O	nd	nd	nd	nd	nd	0.55	0.5	na	na	nd	nd	nd	0.7	nd	0.0
total	100.0	100.0	99.95	99.05	100.7	99.65	98.7	100.1	98.8	100.35	100.0	100.1	100.8	100.1	101.0
Si	2.02	2.03	1.99	1.98	1.98	1.97	1.98	1.99	1.99	1.99	1.98	1.98	1.96	2.00	1.50
Al			0.01	0.02	0.02	0.03	0.02	0.01	0.01	0.01	0.02	0.02	0.04		0.01
Al	0.02	0.05	0.01	0.01		0.03	0.04	0.07	0.04	0.02	0.04	0.03	0.02	0.04	
Ti	0.00	0.00	0.00	0.01	0.01	0.01	0.005	0.00	0.00	0.00	0.00	0.00	0.005	0.00	0.00
Fe^{2+}	0.80	0.75	1.59	1.46	1.50	0.84	0.80	1.17	1.50	1.54	0.75	0.71	0.76	1.52	2.66
Mn	0.01	0.01	0.04	0.03	0.03	0.01	0.015			0.04	0.02	0.02	0.015	0.04	0.05
Mg	0.28	0.25	0.32	0.46	0.42	0.35	0.34	0.37	0.425	0.37	0.35	0.31	0.35	0.33	0.26
Ca	0.84	0.85	0.04	0.04	0.04	0.74	0.77	0.37	0.03	0.05	0.84	0.91	0.82	0.04	0.005
Na	0.00	0.00	0.00	0.00	0.00	0.04	0.04			0.00	0.00	0.00	0.05	0.00	0.00
total	3.97	3.94	4.00	4.01	4.00	4.02	4.01	3.98	3.995	4.02	4.00	3.98	4.02	3.97	4.485
En	14.6	13.5	16.4	23.5	21.4	18.1	17.8	19.4	21.7	18.9	18.0	16.1	18.1	17.5	Fo 8.9
Fs	41.7	40.5	81.5	74.5	76.5	43.5	41.9	61.2	76.7	78.6	38.7	36.8	39.4	80.4	Fa 91.1
Wo	43.7	46.0	2.1	2.0	2.1	38.4	40.3	19.4	1.6	2.5	43.3	47.1	42.5	2.1	
Fe/(Fe+Mg)	0.74	0.75	0.83	0.76	0.78	0.70	0.70	0.76	0.78	0.81	0.68	0.70	0.68	0.82	
N	1	10	2	2	2	2				5	3	6		1	

Notes. Structural formulae are calculated to 6 oxygens. SAMPLE R 394: SOLIDUS: 1 orthopyroxene overgrowth on augite; 2 ditto at the contact with augite; 3 bulk inverted pigeonite; 4 recalculated solidus composition of augite; 5 bulk analysis of solidus augite. STAGE 1: 6 augite, including OI lamellae; 7 matrix near PI'100'; 8 matrix, including OI and OII lamellae; 9 bulk analysis of PI'001' lamellae; 10 recalculated comp. of PI'001' before inversion ; 11 bulk analysis of PI'100' lamella; 12 orthopyroxene matrix of PI'100'; 13 (100) augite lamellae in PI'001'; 14 orthopyroxene matrix in PI'100'. STAGE 2: 15 OI lamellae; 16 matrix. STAGE 3: 17 matrix; 18 PII'001'. OLIVINE 87% Fa (estimated from 2V). SAMPLE R 340: SOLIDUS: 1 stubby, prismatic primary orthopyroxene; 2 orthopyroxene overgrowth on augite; 3 recalculated solidus compositions of augite. STAGE 1: 4 matrix; 5 bulk PI'001' lamellae. STAGE 2: 7 OI lamella; 8 matrix between closely spaced OI and OII lamellae. STAGE 3: 9 matrix after precipitation of OI, OII and PII; 10 matrix between PIa and PII lamellae; 11 PII lamellae. OLIVINE: 12.

Analytical details. Electron microprobe data (*) by FJMR (data for P 340 taken from Rietmeijer, 1979, where procedure and accuracy are described). Analytical electron microscope analyses (**) by G. Cliff, University of Manchester. 'nd' - not detected; 'na' - not analysed; N - number of analyses. 'Bulk' analyses were obtained by scanning the grain using a beam of diameter about 5 microns. *'Recalculated' analyses* were obtained from other analyses in the table and estimated, relative amounts of subsolidus phases (from optical and electron optical micrographs).

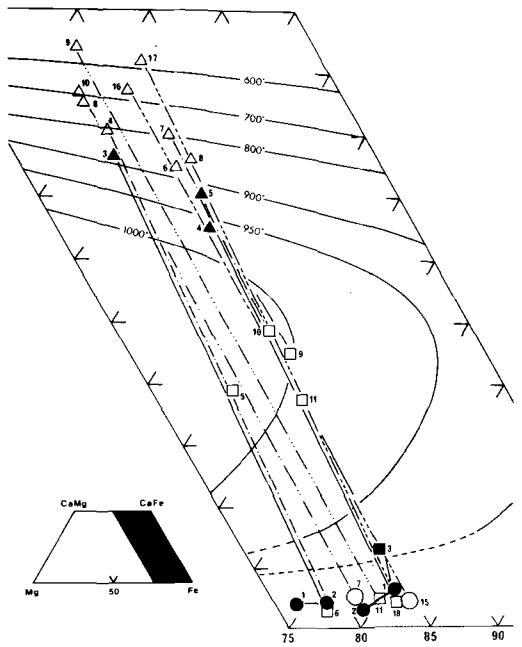

FIG. 9. Plot on the pyroxene quadrilateral of the solidus and subsolidus pyroxene analyses in Table 2. Circles: orthopyroxenes; squares: Ca-poor clinopyroxenes; triangles: Ca-rich clinopyroxenes. Closed symbols represent solidus compositions and open symbols represent subsolidus compositions. Solidus tie-lines: solid lines; subsolidus tie-lines: dot-dashed lines. The number of dots corresponds to the subsolidus stage. The isothermal projections of the pig-aug. and opx-aug. solvi are from Ross and Huebner (1975). Note: analyses 12, 13, and 14 for R394 have been omitted from the figure because they are from phases exsolved within existing PI lamellae. Olivine analyses have also been excluded.

fig. 9. It is notable that the compositions of the OI, PII, and PIII lamellae and the orthopyroxene components of PI '001' and PI '100' are identical within experimental error. Thus the precipitates, although they nucleated at different temperatures, continued to exchange solute with the matrix until roughly the same temperature was reached. (There must be a slight difference in the composition of the pigeonite and orthopyroxene phases, with the latter being poorer in Ca, because the stable and metastable solvi do not coincide. However, the analyses are not sufficiently accurate to detect this.)

Investigation of the subsolidus trends in the Skaergaard and Bushveld intrusions (Coleman, 1978; Nobugai *et al.*, 1978; Buchanan, 1979) has shown that there is a change during cooling not only in the Ca:(Fe+Mg) ratio of the phases, but also in the Fe:Mg ratio. In all cases the Fe:Mg ratio increased in the Ca-poor phase and decreased in the Ca-rich phase, i.e. there was an anticlockwise rotation of the tie-lines with decreasing temperature. The effect was less marked for the Bushveld than for the Skaergaard intrusion. Nobugai *et al.*, 1978 suggested that chemical changes took place in two stages; first the diffusion between Ca and (Fe+Mg) ions kept the Fe/Mg ratio nearly constant. In the second stage diffusion of Ca virtually ceased and the matrix and lamellae exchanged Mg and Fe.

In fig. 9 there is no evidence of a rotation of the tie-lines. It may be that, if cooling is slow enough and equilibrium is maintained, no tie-line rotation occurs, whatever the composition of the primary phases. On the other hand it is possible that tie-line rotation is less marked the higher is the Fe content of the pyroxenes.

Pyroxene geothermometry

Solidus equilibrium. We have used three methods to estimate the solidification temperature of the pyroxenes in R394. Ross and Huebner (1975) presented isothermal projections of the pseudo-binary pyroxene *T-X* (Wo) diagram on to the pyroxene quadrilateral for zero–5 kbar. An inventory of available data tentatively shows that the results of Ross and Huebner (1975) remain virtually unchanged up to about 10 kbar, at least for iron-rich compositions (Rietmeijer, 1979). The chemical data for sample R394 (fig. 9) indicate that the Ca-poor pyroxenes solidified at about 950 °C and that the Ca-rich pyroxene solidified at a somewhat higher temperature. This is in contrast to the textural evidence which, as mentioned earlier, suggests that solidification occurred close to the three-phase field. However, the isothermal projections of Ross and Huebner must be treated with caution when applied to natural pyroxenes as the experiments were carried out on pure phases.

Several authors have attempted to develop the exchange of Fe–Mg between coexisting orthopyroxene and Ca-rich clinopyroxene at different temperatures as a geothermometer. Kretz (1963) showed that the distribution coefficient $K_{D(Fe-Mg)} = (Fe^{2+}/Mg)_{opx}/(Fe^{2+}/Mg)_{cpx}$ for solidus ortho- and clinopyroxenes could be used to distinguish between igneous and metamorphic pairs. He also suggested that there is an approximately linear relationship between $\ln K_{D(Fe-Mg)}$ and $1/T$. Kretz's method gives values of 1110 °C and 1135 °C for the temperatures of solidification of R394 and R340 respectively (Table III), estimates that must be too high.

The equations of Wood and Banno (1973) and Wells (1977) are more sophisticated expressions than Kretz's of the relationship between K_D and

temperature for orthopyroxene /Ca-clinopyroxene pairs. Wood and Banno's equation gives solidification temperatures for the pyroxenes of 874 °C ± 70 for R394 and 830 °C ± 70 for R340; Well's equation gives 945 °C and 894 °C respectively (Table III).

Ishii (1975) showed that the minimum temperature of stability of pigeonite at one atmosphere (the 'pigeonite eutectoid reaction line', i.e. the temperature at which augite, orthopyroxene, and pigeonite coexist) is related to the Fe/Mg ratio of the pigeonite by the equation:

$$T(°C) \sim 1270 - 480\, X_{Fe}$$

where X_{Fe} is the atomic ratio Fe/(Fe + Mg) in the pigeonite. Solving the equation for sample R394 gives a temperature of 867 °C. However, the minimum temperature of pigeonite stability increases with increasing pressure. Ishii estimated that the effect of pressure is described by the equation:

$$T(°C) \sim 1270 - 480\, X_{Fe} + (10 - 5\, X_{Fe})\, P$$

where P is expressed in kilobars. An assumed value of 9 kbar for P (see below) yields 920 °C for the temperature of equilibration of the pyroxenes. Apart from the results obtained by Kretz's method, the various estimates thus suggest a temperature of approximately 900 °C for R394 and a slightly lower temperature for R340.

The Fe–Mg exchange reaction between coexisting orthopyroxene and olivine may be used to estimate the pressure at which solidification took place if the temperature is known. Frisch and Bridgwater (1976) showed that:

$$468.0 = -1.9873\, T \ln (X_{opx}/X_{ol}) + 39P$$

where T is in °K, P is in kilobars and the X's are as above. Assuming a temperature of 900 °C for sample R394 and 850 °C for sample R340 gives pressures for these rocks of 9.2 and 3.1 kbar respectively. This large difference in pressures is surprising because both samples come from the same layer of the complex. It is therefore unlikely that conditions of solidification could have varied that much. It is possible that the difference in calculated pressures is a reflection of different conditions of re-equilibration in the subsolidus. However, Sack (1980) has pointed out that, because of our incomplete knowledge of intra- and intergranular parameters for the exchange reaction, thermodynamic formulations for the exchange between orthopyroxene and olivine should be regarded with caution.

In the iron-rich portion of the pyroxene quadrilateral the breakdown reaction of Ca-poor pyroxene to less Fe- and Ca-rich orthopyroxene + Fe-rich olivine + quartz ± ferroaugite (Lindsley and

TABLE III. Temperature estimates for coexisting solidus and subsolidus pyroxene phases as estimated using various geothermometers

Sample	Phase I	Phase J	$K_{D(Fe-Mg)}^{I-J}$	$1/K_D$	T°C (Kretz)	T°C (Wood/Banno)	T°C (Wells)	T°C (Robinson et al.)	
R394	1	4	1.35	0.74	1146	882	950		solidus pair(s)
	1	5	1.41	0.71	1075	866	938		
								850-750	stage 1
	15	16	1.88	0.53	647	850	910	-	stage 2
	18	17	1.66	0.60	813	813	856	600-400	stage 3
R340	1	3	1.28	0.78	1237	822	883		solidus pair(s)
	2	3	1.45	0.69	1032	839	905		
								800(-650)	stage 1
	7	8	1.94	0.51	600	841	904	-	stage 2
	11	9	2.01	0.50	576	769	793	600-400	stage 3

The numbers I and J correspond to the numbers of analyses in Table 2. The estimated error in the Wood/Banno and Wells geothermometers is ± 70° (Wood and Banno, 1973; Wells, 1977). The K_D-value for the 810°- isotherm in the pyroxene quadrilateral is 1.45 (Lindsley et al., 1974).

Munoz, 1969; Smith, 1971, 1972, 1974) may be used to estimate P-T conditions. Isopleths for the breakdown reaction (compositions Fs_{70-100}) in a P-T diagram have been constructed by Jaffe *et al.* (1978). Taking the $\alpha \rightarrow \beta$ quartz transition into account Bohlen *et al.* (1980) re-evaluated the nature of isopleths for compositions Fs_{90-100}. In rocks from the 'Leuconoritic Phase' of the Bjerkreim-Sokndal lopolith the breakdown reaction is not observed (Rietmeijer, 1979) and the isopleth for the most Fe-rich Ca-poor pyroxene (R394: Fs_{84}) sets a minimum for the total pressure for a given temperature; for a temperature of about 900 °C P_{total} is greater than about 8 kbar.

Subsolidus equilibrium. Although they were originally calibrated for solidus Fe-Mg exchange between coexisting ortho- and clinopyroxene pairs, pyroxene geothermometers have been used to estimate the equilibration temperatures of subsolidus pyroxene pairs, both ortho-clino and clino-clino (Nobugai *et al.*, 1978). The temperatures obtained using the various geothermometers on R394 and R340 are shown in Table III.

As noted above, the compositions of the precipitates in stages 2, 3, and 4 are identical within experimental error. Thus the variation shown in the estimated temperatures of equilibration for stages 2 and 3 is merely a reflection of this error. However, the temperatures are too high,[1] particularly those calculated with the Wood/Banno and Wells geothermometers. It seems unlikely that all equilibration took place above about 800 °C within the Rogaland pyroxenes when temperatures for nucleation of phases visible in the optical microscope in more Mg-rich pyroxenes from the Bushveld intrusion were much lower than this (Robinson *et al.*, 1977).

Modelling of cell parameters

We have used the orientation of the interfaces of exsolution lamellae, as proposed by Robinson *et al.* (1977), to estimate the temperatures of exsolution. Published relations between the unit-cell parameters, a, c, and β and temperature for diopside and hedenbergite (Cameron *et al.*, 1973) and for clinohypersthene $En_{31}Fs_{67}Wo_2$ (Smyth and Burnham, 1972; Smyth, 1974), together with single points for low clinoferrosilite (Burnham, 1965) and high clinoferrosilite (Sueno, pers. comm.), were plotted. Room-temperature cell dimensions for clinopyroxenes Wo_0 and W_{50} on the tie-line for R394 were taken from Turnock *et al.* (1973) and extrapolated to higher temperatures using the curves already plotted. Fortunately the compositions of the primary pigeonites are quite close to the composition of the clinohypersthene for which the most detailed, accurate cell parameters are available. These data, together with the room-temperature parameters for clinopyroxenes Wo_{5-45} on the R394 tie-line as calculated from the data of Turnock *et al.* (1973), were used to model the variation of cell parameters a, c, and β with temperature for the clinopyroxenes of R394 (fig. 10). The data of Ross *et al.* (1973) for ferro-augite were used to estimate the position of the coherent solvus in the T-X(Wo) diagram. The orientations for the '001' and '100' lamellar interfaces were calculated as a function of temperature using the modelled cell parameters appropriate to the strain-free solvus (fig. 11). The model angles, together with Table I, suggest that PI '100' and '001' lamellae (stage 1) nucleated at 850-750 °C, and PII (stage 3) nucleated between about 600 and 400 °C. The range of angles for the very late-stage PIII lamellae lies partly outside the calculated values and we conclude that the model is not reliable for low temperatures. Apart from those for PIII, the temperatures for nucleation of the various exsolutions show reasonable values, unlike those derived from the K_D values and the geothermometers.

Discussion

The very slow rates of cooling deduced by Rietmeijer and Heijnen (in prep.) are consistent with the lengths of the tie-lines between matrix and precipitate phases. The estimates of temperatures of nucleation obtained from the orientation of the habit planes of the exsolution lamellae give very reasonable values, except for the very late-stage PIII lamellae. (Champness and Lorimer (1982) found that estimates of exsolution temperatures for the last set of pigeonite lamellae in an augite from the Bushveld intrusion were also too low.) The reason for the unreliability of the geothermometer at low temperatures is probably twofold. First, its accuracy will be greatest in the temperature range for which the cell parameters of pigeonite are changing most rapidly. In the case of the Rogaland pyroxenes this occurs between about 600-800 °C for the a-axis and 700-800° for the c-axis and β. Thus the estimates of the '100' angles are more affected than the '001' angles at low temperatures. (They are determined by $(c_p-c_a)/c_a$ and $\beta_p-\beta_a$, where p and a refer to pigeonite and augite respectively.) Secondly, and more importantly, the solvus that was used to estimate the compositions of the coexisting phases was only determined for temperatures down to 850 °C and for a single point at 25 °C (which had a large error bar, Ross *et al.*, 1973). We

[1] The unrealiability of geothermometers at low temperatures has been discussed by, among others, Bohlen and Essene (1979), Blander (1972), and Roeder *et al.* (1980).

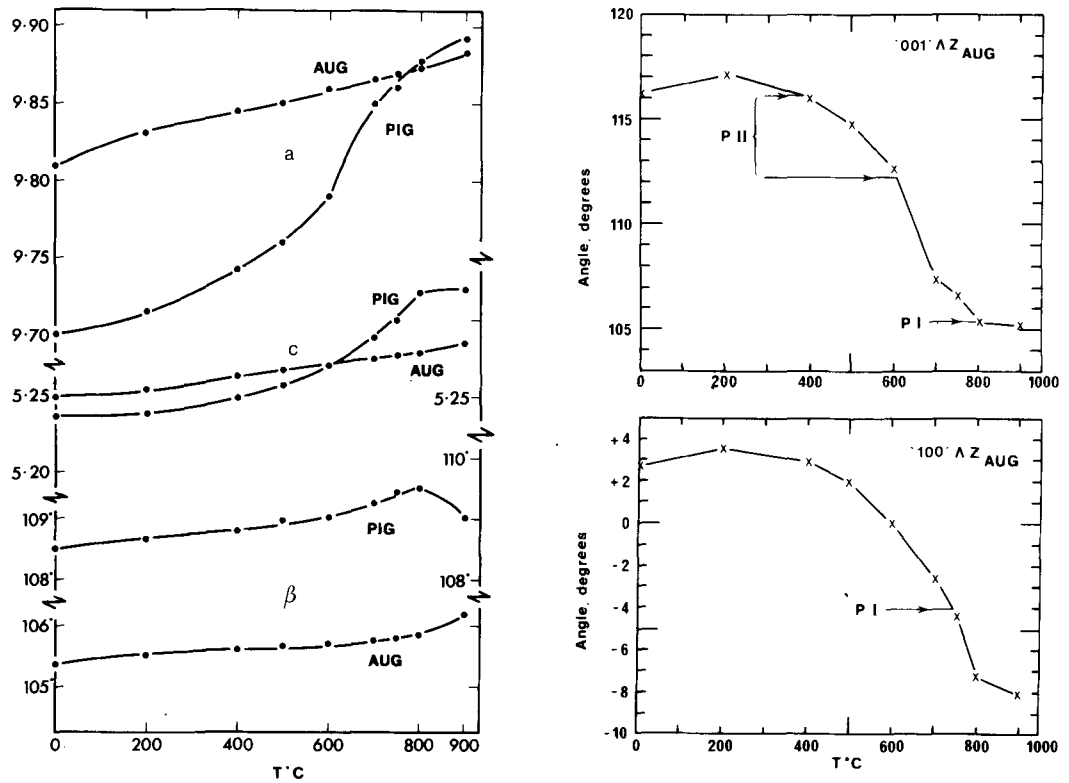

FIGS. 10 and 11. FIG. 10 (*left*). Modelled cell parameters for the join En:Fs = 15:85 for the pyroxenes from R394. The compositions have been estimated from the 'ferro-augite' solvus of Ross *et al.* (1973) and the temperature of the C → P transition in pigeonite was estimated from the data of Prewitt *et al.* (1971). FIG. 11 (*right*). Calculated orientations of the '001' and '100' pyroxene lamellae in R394 as a function of temperature.

thus had to extrapolate the solvus between 850 and 25 °C.

However, despite the present limitations of Robinson *et al.*'s method, it is potentially a very powerful geothermometer because the physical principles involved are well understood. Accurate cell dimensions at different temperatures for representative pyroxenes across the quadrilateral and accurate subsolidus phase diagrams are now required to improve the accuracy of the geothermometer.

Acknowledgements. Part of this research was carried out while F.J.M.R. was supported by a grant from the Netherlands Organization for the Advancement of Pure Research (ZWO). F.J.M.R. also wishes to thank the Departments of Geology and Metallurgy, University of Manchester for the hospitality and facilities provided during his visits. Electron microprobe analyses were carried out by F.J.M.R. at the Vening Meinesz Laboratory of Geophysics and Geochemistry, Rijksuniversiteit, Utrecht and thin-film analyses were performed by Mr G. Cliff (University of Manchester) to whom we are particularly indebted. We wish to thank Dr G. W. Lorimer for helpful discussions. P.E.C. acknowledges grants GR3/1634 and 3580 from the Natural Environment Research Council of Great Britain.

REFERENCES

Blander, M. (1972) *Geochim. Cosmochim. Acta*, **36**, 787.
Bohlen, S. R., and Essene, E. J. (1979) *Lithos*, **12**, 335.
——and Boettcher, A. L. (1980) *Earth Plan. Sci. Lett.* **47**, 11.
Buchanan, D. L. (1979) *J. Petrol.* **20**, 327.
Burnham, C. W. (1965) *Carnegie Inst. Washington Yearb.* **64**, 202.
Buseck, P. R., and Iijima, S. (1975) *Am. Mineral.* **60**, 771.
——Nord, G. L., *Jr.*, and Veblen, D. R. (1980) *Reviews in Mineralogy*, **7**, Mineral. Soc. Am. 117.
Cameron, M., Sueno, S., Prewitt, C. T., and Papike, J. J. (1973) *Am. Mineral.* **58**, 594.
Champness, P. E., and Copley, P. A. (1976) In *Electron Microscopy in Mineralogy* (H.-R. Wenk, ed.), Springer-Verlag, 228.

Champness, P. E., and Lorimer, G. W. (1982) In *Interphase Boundaries in Solids* (G. A. Chadwick and D. A. Smith, eds.), Academic Press. In press.
——Cliff, G., and Lorimer, G. W. (1981) *Bull. Minéral.* **104,** 236.
Coleman, L. C. (1978) *Contrib. Mineral. Petrol.* **66,** 221.
Frisch, T., and Bridgwater, D. (1976) Ibid. **57,** 25.
Hermans, G. A. E. M., Tobi, A. C., Poorter, R. P. E., and Maijer, C. (1975) *Nor. Geol. Unders.* **318,** 51.
Huebner, J. J. (1980) *Reviews in Mineralogy*, **7,** Mineral. Soc. Am., 213.
Isaacs, A. H., and Peacor, D. R. (1981) *EOS* **62,** 434.
Ishii, T. (1975) *Mineral J. Japan.* **8,** 48.
Jaffe, H. W., Robinson, P. R., Tracy, R. J., and Ross, M. (1975) *Am. Mineral.* **60,** 9.
————(1978) Ibid. **63,** 1116.
Kars, H., Jansen, J. B. H., Tobi, A. C., and Poorter, R. P. E. (1980) *Contrib. Mineral. Petrol.* **74,** 235.
Kretz, R. (1963) *J. Geol.* **71,** 773.
Lindsley, D. H., and Munoz, J. L. (1969) *Am. J. Sci.* **267-A,** 295.
——King, H. E., *Jr.*, and Turnock, A. C. (1974) *Geophys. Res. Lett.* **1,** 134.
McCallister, R. H., and Nord, G. L., *Jr.* (1981) *Am. Mineral.* In press.
McLaren, A. C., and Etheridge, M. A. (1976) *Contrib. Mineral. Petrol.* **57,** 163.
Michot, J., and Michot, P. (1969) *N.Y. State Museum and Sci. Service, Mem.* **18,** 399.
Nakajima, Y., and Hafner, S. S. (1980) *Contrib. Mineral. Petrol.* **72,** 101.
Nobugai, K., and Morimoto, N. (1979) *Phys. Chem. Minerals*, **4,** 361.
——Tokonami, M., and Morimoto, N. (1978) *Contrib. Mineral. Petrol.* **67,** 111.
Nord, G. L., *Jr.*, and McGee, J. J. (1979) *Proc. Lunar. Planet. Sci. Conf. 10th*, 817.
Prewitt, C. T., Brown, G. E., and Papike, J. J. (1971) *Proc. Lunar Planet. Sci. Conf. 2nd* **1,** 59.
Rietmeijer, F. J. M. (1979) *Pyroxenes from iron-rich igneous rocks in Rogaland, S.W. Norway.* Geol. Ultraiectina 21, 341 pp.
——and Champness, P. E. (1980*a*) *Proc. 7th Eur. Cong. Electron Microscopy*, The Hague, **1,** 452.
————(1980*b*) *Inst. Phys. Conf. Ser.* No. 52, 105.
Robinson, P., Jaffe, H. W., Ross, M., and Klein, C., *Jr.* (1971) *Am. Mineral.* **56,** 909.
——Ross, M., Nord, G. L., *Jr.*, Smyth, J. R., and Jaffe, H. W. (1977) Ibid. **62,** 857.
Roeder, P., Campbell, I. H., and Jamieson, H. (1980) *Contrib. Mineral. Petrol.* **23,** 205.
Ross, M., and Huebner, J. S. (1975) *Extended abstracts, Int. Conf. Geothermometry Geobarometry*, Pennsylvania State Univ.
——Robinson, P., and Jaffe, H. W. (1972) *Geol. Soc. Am. Abstr. with Programs*, **4,** 644.
——Huebner, J. S., and Dowty, E. (1973) *Am. Mineral.* **58,** 619.
Sack, R. O. (1980) *Contrib. Mineral. Petrol.* **71,** 257.
Smith, D. (1971) *Am. J. Sci.* **271,** 370.
——(1972) *Am. Mineral.* **57,** 1413.
——(1974) *J. Petrol.* 15, **58.**
Smyth, J. R. (1974) *Am. Mineral.* **59,** 1069.
——and Burnham, C. W. (1972) *Earth Planet. Sci. Lett.* **14,** 183.
Turnock, A. C., Lindsley, D. H., and Grover, J. E. (1973) *Am. Mineral.* **58,** 50.
Verschure, R. H., Andriessen, P. A. M., Beolrijk, N. A. I. M., Hebeda, E. H., Maijer, C., Priem, H. N. A., and Verdurmen, E. A. Th. (1980) *Contrib. Mineral. Petrol.* **74,** 245.
Wells, P. R. A. (1977) Ibid. **62,** 129.
Wood, B. J., and Banno, S. (1973) *Contrib. Mineral. Petrol.* **42,** 109.